(12) R. B. Shibaeva and L. O. Atovmyan, *J. Struct. Chem. (Engl. Transl.)*, **13**, 514 (1972).
(13) F. H. Herbstein, *Perspect. Struct. Chem.*, **4**, 269 (1971).
(14) Z. G. Soos, *Annu. Rev. Phys. Chem.*, **24**, 121 (1974).
(15) D. J. Dahm, P. Horn, G. R. Johnson, M. G. Miles, and J. D. Wilson, *J. Cryst. Mol Struct.*, **5**, 27 (1975).
(16) J. S. Miller and A. L. Balch, *Inorg. Chem.*, **11**, 2069 (1972).
(17) J. C. Scott, Ph.D. Thesis, University of Pennsylvania, 1975.
(18) "International Tables for X-Ray Crystallography", Vol. I, Kynoch Press, Birmingham, England, 1969.
(19) The programs for refinement of lattice constants and automated operation of the diffractometer are those of Busing and Levy as modified by Picker Corporation.
(20) All computations were carried out on an IBM 360/65 computer. Cell reduction was done using Lawton's TRACER II. Locally modified versions of the following programs were used: Raymond's URFACS for data reduction; Ibers' NUCLS, a group least-squares version of the Busing–Levy ORFLS program; Zalkin's FORDAP Fourier program; ORFFE, a function and error program by Busing, Martin, and Levy; Johnson's ORTEP2 thermal ellipsoid plotting program. A number of local programs were also used.
(21) T. C. Furnas, "Single Crystal Orienter Instruction Manual", General Electric Co., Milwaukee, Wis., 1957.
(22) W. R. Busing and H. A. Levy, *J. Chem. Phys.*, **26**, 563 (1957).
(23) D. T. Cromer and B. Mann, *Acta Crystallogr., Sect. A*, **24**, 321 (1968).
(24) D. T. Cromer and D. Lieberman, *J. Chem. Phys.*, **53**, 1891 (1970).
(25) R. F. Stewart, E. R. Davidson, and W. T. Simpson, *J. Chem. Phys.*, **42**, 3175 (1965).
(26) $R_1 = \Sigma||F_o| - |F_c||/\Sigma|F_o|$; $R_2 = [\Sigma w(|F_o| - |F_c|)^2/\Sigma w|F_o|^2]^{1/2}$; estimated standard deviation of an observation of unit weight = $[\Sigma w(|F_o| - |F_c|)^2/(N_o - N_v)]^{1/2}$ where N_o and N_v are the number of observations and variables, respectively.
(27) See paragraph at end of paper regarding supplementary material.
(28) S. Otsuka, Y. Tatsuna, and M. Miki, *J. Chem. Soc. Chem. Commun.*, 445 (1973).
(29) D. J. Doonan, A. L. Balch, S. Z. Goldberg, R. Eisenberg, and J. S. Miller, *J. Am. Chem. Soc.*, **97**, 1961 (1975); S. Z. Goldberg and R. Eisenberg, *Inorg. Chem.*, **15**, 535 (1976).
(30) W. M. Butler and J. H. Enemark, *Inorg. Chem.*, **12**, 540 (1973).
(31) W. M. Butler, J. H. Enemark, J. Parks, and A. L. Balch, *Inorg. Chem.*, **12**, 451 (1973).
(32) (a) B. Jovanovic and Lj. Manojlovic-Muir, *J. Chem. Soc., Dalton Trans.*, 1176 (1972); (b) B. Jovanović, Lj. Manojlovic-Muir, and K. W. Muir, *ibid.*, 1178 (1972).
(33) C. J. Fritchie, Jr., and P. Arthur, Jr., *Acta Crystallogr.*, **21**, 139 (1966).
(34) (a) H. Kobayashi, Y. Ohashi, F. Marumo, and Y. Saito, *Acta Crystallogr., Sect. B*, **26**, 459 (1970); (b) H. Kobayashi, T. Danno, and Y. Saito, *Acta Crystallogr., Sect. B*, **29**, 2693 (1973).
(35) (a) H. T. Jonkman and J. Kommandeur, *Chem. Phys. Lett.*, **15**, 496 (1972); (b) J. L. de Boer and A. Vos, *Acta Crystallogr., Sect. B*, **28**, 835 (1972), and references therein.
(36) P. Goldstein, K. Seff, and K. N. Trueblood, *Acta Crystallogr., Sect. B*, **24**, 778 (1968).
(37) R. E. Long, R. A. Sparks, and K. N. Trueblood, *Acta Crystallogr.*, **18**, 932 (1965).
(38) A. Hoekstra, T. Spoelder, and A. Vos, *Acta Crystallogr., Sect. B*, **28**, 14 (1972).
(39) A. W. Hanson, *Acta Crystallogr., Sect. B*, **24**, 768 (1968).
(40) T. J. Kistenmacher, T. E. Phillips, and D. O. Cowan, *Acta Crystallogr., Sect. B*, **30**, 763 (1974); T. E. Phillips, T. J. Kistenmacher, J. P. Ferraris, and D. O. Cowan, *J. Chem. Soc., Chem. Commun.*, 471 (1973).
(41) F. Denoyer, R. Comes, A. F. Garito, and A. J. Heeger, *Phys. Rev. Lett.*, **35**, 445 (1975).
(42) T. Sundaresan and S. C. Wallwork, *Acta Crystallogr., Sect. B*, **28**, 2474 (1972).
(43) H. C. Montgomery, *J. Appl. Phys.*, **42**, 2971 (1971).
(44) J. C. Scott, A. F. Garito, and A. J. Heeger, *Phys. Rev. B*, **10**, 3131 (1974).
(45) R. C. Weast, Ed., "Handbook of Chemistry and Physics", 53d ed, Chemical Rubber Co., Cleveland, Ohio, 1972, p E-114.
(46) J. Lewis and R. G. Wilkins, Ed., "Modern Coordination Chemistry", Interscience, New York, N.Y., 1960, p 403. Values for P and F are −26.3 and −6.3 × 10^{-6} emu/(g atom), respectively.
(47) (a) Y. Iida, *Bull. Jpn. Chem. Soc.*, **42**, 71, 367 (1969); (b) Y. Oohashi and T. Sakata, *ibid.*, **46**, 330 (1973).
(48) J. B. Torrence, B. A. Scott, and F. B. Kaufman, *Solid State Commun.*, **17**, 1369 (1975).
(49) J. S. Miller and D. G. Marsh, unpublished results.
(50) H. Isci and W. R. Mason, *Inorg. Chem.*, **14**, 913 (1975).

Metal to Ligand Charge-Transfer Spectra in Tetra-*n*-butylammonium Dicyanoaurate(I)

W. Roy Mason

Contribution from Department of Chemistry, Northern Illinois University, DeKalb, Illinois 60115. *Received December 22, 1975*

Abstract: Electronic absorption spectra at 1.6 K are reported for thin polycrystalline films of $[(n\text{-}C_4H_9)_4N][Au(CN)_2]$ on quartz plates, together with some polarized spectra at 300 K for oriented single crystals grown on quartz or LiF plates. The 1.6 K spectra reveal considerable structure in the major band systems which are observed in the region 40–53 kcm^{-1}. The spectra of the single crystals show strong polarization in the ultraviolet region 40–47 kcm^{-1} and in the infrared cyanide stretching region (2150–2130 cm^{-1}). The structured bands in the 1.6 K spectra are assigned as allowed metal to ligand charge-transfer (MLCT) transitions (Au 5d → π^*CN^-) accompanied by vibrational excitation. Several progressions in the totally symmetric ν_1 (CN stretch) and ν_2 (AuC stretch) modes are identified and electronic origins are tentatively located. The polarized spectra allow differentiation of transitions to allowed Σ_u^+ states (z-polarized) and Π_u states (xy-polarized) below 47 kcm^{-1}. Electronic excited states for $Au(CN)_2^-$ are interpreted by means of a model which includes spin-orbit coupling in MLCT excited configurations, and the results are discussed in terms of 5d-orbital participation in bonding.

The linear $Au(CN)_2^-$ ion is one of the most stable and best structurally characterized two-coordinate complexes known.[1] Solid salts consist of discrete, linear ions, and in solution the complex has virtually no tendency to increase its coordination number beyond two. Indeed, $Au(CN)_2^-$ may be considered as a prototype of linear, two-coordinate complexes containing π acceptor ligands, and as such, there is considerable interest in its electronic structure and spectra.

Recently, solution electronic absorption and magnetic circular dichroism (MCD) spectra for $Au(CN)_2^-$ were reported[1] together with some low temperature (40 K) spectra for $[(n\text{-}C_4H_9)_4N][Au(CN)_2]$, deposited as a thin solid film on quartz. The ion, especially in the solid, exhibits remarkably rich electronic spectra with numerous intense bands observed in the ultraviolet region between 40 and 54 kcm^{-1}. These bands have been assigned[1-3] to metal to ligand charge transfer (MLCT) transitions from the occupied orbitals which are mainly Au 5d to empty ligand based π^* orbitals. While the MLCT assignment seems firm, the detailed assignment of individual transitions among the numerous spectral features remains a complicated and challenging problem. In an effort to solve this problem, the present paper reports some spectral measurements on solid $[(n\text{-}C_4H_9)_4N][Au(CN)_2]$ at 1.6 K and some polarized spectra for oriented crystals at room temperature in the energy region below 47 kcm^{-1}. The 1.6 K spectra show enhanced resolution over the previous 40 K spectra,[1] while band polarizations allow a more precise description of the symmetries of the low lying excited states. The spectra are

interpreted by a model which involves a single π^*CN^- orbital in excited configurations and allows for spin-orbit coupling between the allowed MLCT excited states.

Experimental Section

Tetra-*n*-butylammonium dicyanoaurate(I), $[(n\text{-}C_4H_9)_4N][Au(CN)_2]$, was prepared from the potassium salt[4] and characterized as described previously.[1] The colorless solid melts at 74–75 °C and can be crystalized from water, acetonitrile, absolute ethanol, or aqueous ethanol (1:3 by vol.). Samples for spectral measurements were prepared by slow evaporation at room temperature of concentrated acetonitrile or ethanol solutions of $[(n\text{-}C_4H_9)_4N][Au(CN)_2]$ on optical quality quartz or lithium fluoride plates. Very thin (<1 μ) crystals were produced in this manner, some as large as 3 × 5 mm. Thicker single crystals suitable for x-ray photographs were grown by slow evaporation from water or aqueous ethanol at room temperature.

Crystal Data.[5] From single-crystal x-ray diffraction, together with Weissenberg and precession photographs, $[(n\text{-}C_4H_9)_4N][Au(CN)_2]$ was determined to be monoclinic with space group $C2/c$. The unit cell contains four formula units and has dimensions: a = 9.301 (8) Å, b = 13.108 (9) Å, c = 19.189 (17) Å, and β = 97.55 (5)°. The calculated density (1.407 g cm^{-3}) agrees favorably with that determined by floatation in bromobenzene (1.45 g cm^{-3}). The complete crystal structure will be published elsewhere;[6] however, some details pertinent to the present study may be noted here. The gold atoms lie at inversion centers located at the fourfold special positions (¼, ¼, 0) and (¾, ¼, ½). The linear ions are parallel to one another and are nearly parallel to the *ac* plane (perpendicular to the twofold *b* axis), and the ions make an angle of approximately 67° with the *a* axis. The closest Au–Au distance is 8.04 Å.

The crystals grown from aqueous solution or aqueous ethanol develop as thin transparent plates, usually elongated along the *a* axis, with the plate face [001]. Parallel extinctions are observed when incident light is perpendicular to the plate face. The thin crystals grown on optical plates developed in elongated fan shaped clusters with no well-developed faces. However, sharp extinctions were observed parallel and perpendicular to the direction of elongation. An x-ray powder pattern of the thin crystals grown on optical plates was identical with that of the thicker crystals used for the single-crystal x-ray studies.

Spectral Measurements. Electronic spectra were obtained using either a Cary 14 or a Cary 1501 spectrophotometer. The spectral slit widths were generally less than 50 cm^{-1} throughout the spectral region of measurement. Low temperature spectra were obtained using a glass Dewar fitted with quartz windows. The samples were immersed in liquid helium which was cooled below the λ point by pumping. It was not possible to measure single-crystal polarized spectra at low temperatures because the thin crystals, which adhere strongly to the optical plates, cracked and became polycrystalline (differences in thermal expansion coefficients between the fragile crystals and the optical plates are likely responsible for this difficulty though a crystal phase transition cannot be ruled out). Polarized single-crystal spectra could be obtained at room temperature, however. Samples on optical plates were oriented with the aid of a polarizing microscope and mounted over small slots cut in aluminum foil. Glan-Taylor air spaced calcite polarizers were used in both sample and reference beams of the spectrophotometer; the absorption and birefringence of the optical plates were negligible in the spectral region of interest. Polarized infrared spectra were obtained for crystals grown on lithium fluoride plates, using a Perkin-Elmer 125 spectrophotometer equipped with a wire grid-AgBr polarizer. If the crystals were warmed above ~35° they became polycrystalline. To avoid difficulty when the sample was placed in the infrared beam, cool nitrogen gas was passed over the sample cooling it to about 10°. Samples treated in this way could be recovered unchanged, and several samples were examined in both the infrared and ultraviolet.

Results and Discussion

Molecular Orbital Energy Levels and MLCT Excited States. The one-electron molecular orbital energy levels for linear dicyano complexes have been given previously.[1] A simplified energy level diagram which will be helpful in visualizing the MLCT excitations in $Au(CN)_2^-$ is presented in Figure 1 showing the highest energy occupied "metal" Au 5d orbitals

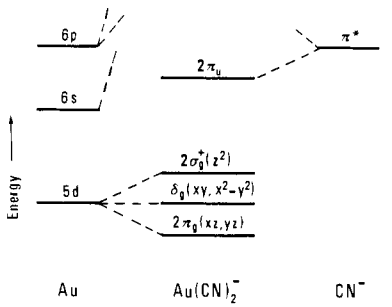

Figure 1. Simplified molecular orbital energy level diagram for $Au(CN)_2^-$.

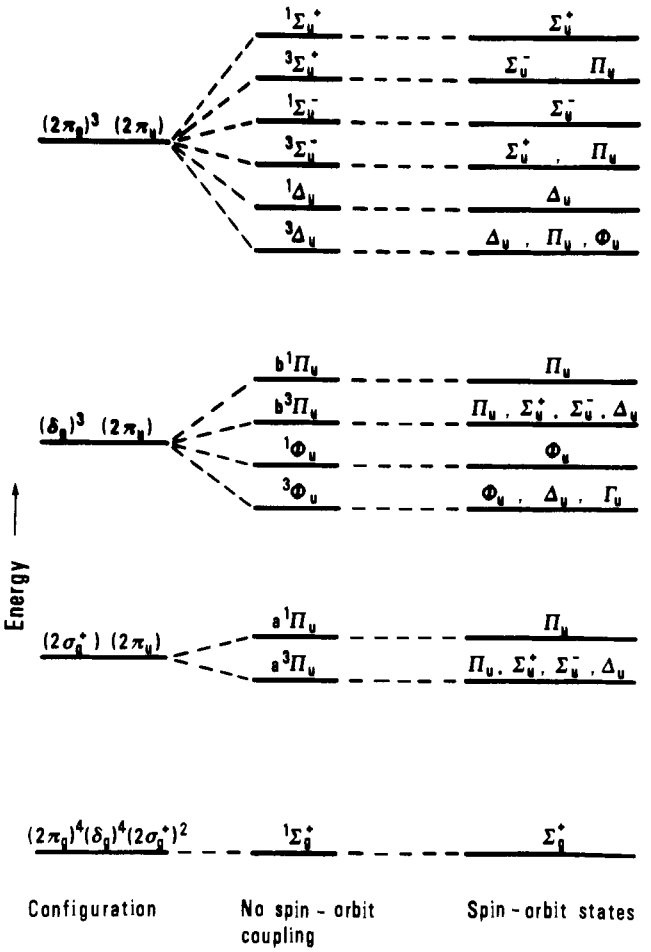

Figure 2. Excited states for MLCT 5d → $2\pi_u(CN^-)$ excitations in $Au(CN)_2^-$.

and the lowest energy unoccupied "ligand" π^* CN^- orbital. The ground electron configuration is $5d^{10}$ so that the complex is diamagnetic and has a nondegenerate, totally symmetric ground state, $^1\Sigma_g^+$. With the molecular axis taken to lie along the z direction, the MLCT states arising from the three 5d → $2\pi_u$ excitations, $2\sigma_g^+(z^2) \rightarrow 2\pi_u$, $\delta_g(xy, x^2-y^2) \rightarrow 2\pi_u$, and $2\pi_g(xz, yz) \rightarrow 2\pi_u$, are shown in Figure 2. Only transitions to $^1\Sigma_u^+$ or $^1\Pi_u$ states are fully allowed by dipole selection rules, the former polarized parallel to the molecular axis (z polarized) and the latter polarized perpendicular to the molecular axis (xy polarized). However, as noted earlier,[1] strong spin-orbit coupling in $Au(CN)_2^-$ (ζ_{5d} for a free Au(I) ion is ca. 5100 cm^{-1} [7]) causes spin selection rules to break down and therefore the MLCT excited states are more appropriately designated by spin-orbit states characterized by double group representations shown on the right hand side of Figure 2 (the double group representations are characterized by the lack of spin

Table I. Spin-Orbit Secular Determinants (upper triangles).

Π_u states

$a^1\Pi_u - E$	0	$(3/8)^{1/2}\zeta$	$-(3/4)^{1/2}\zeta$	$-(3/8)^{1/2}\zeta$	0	0
	$a^3\Pi_u - E$	$-i(3/8)^{1/2}\zeta$	$-i(3/4)^{1/2}\zeta$	$i(3/8)^{1/2}\zeta$	0	0
		$^3\Sigma_u^+ - E$	0	$-\zeta/2$	$-i\zeta/2$	$-\zeta/2$
			$^3\Delta_u - E$	0	0	0
				$^3\Sigma_u^- - E$	$-i\zeta/2$	$-\zeta/2$
					$b^3\Pi_u - E$	$-i\zeta$
						$b^1\Pi_u - E$

Σ_u^+ states

$a^3\Pi_u - E$	$(3/4)^{1/2}\zeta$	$i(3/4)^{1/2}\zeta$	0
	$^1\Sigma_u^+ - E$	$i\zeta/2$	$-(1/2)^{1/2}\zeta$
		$^3\Sigma_u^- - E$	$-i(1/2)^{1/2}\zeta$
			$b^3\pi_u - E$

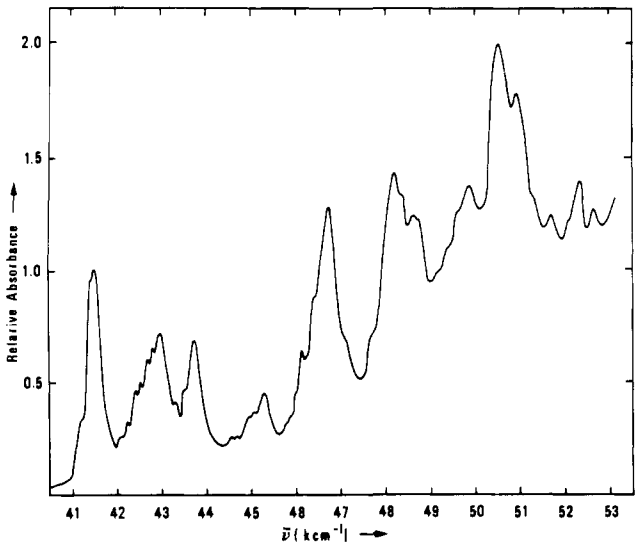

Figure 3. Electronic spectra for a thin polycrystalline film of $[(n\text{-}C_4H_9)_4N][Au(CN)_2]$ on quartz at 1.6 K.

multiplicity superscripts). The wave functions for the spin-orbit states of a given symmetry contain components of the same symmetry from the various singlet and triplet states in the absence of spin-orbit coupling. However, only Σ_u^+ and Π_u states need to be considered to a first approximation, since transitions to Σ_u^-, Δ_u, and Φ_u states are symmetry forbidden. Thus, wave functions for the $\Pi_u(i)$ and $\Sigma_u^+(i)$ states will be given by eq 1 and 2,

$$|\Pi_u(i)\rangle = a_i|(a^1\Pi_u)\rangle + b_i|(a^3\Pi_u)\rangle + c_i|(^3\Sigma_u^+)\rangle + d_i \times |(^3\Delta_u)\rangle + e_i|(^3\Sigma_u^-)\rangle + f_i|(b^3\Pi_u)\rangle + g_i|(b^1\Pi_u)\rangle \quad (1)$$

$$|\Sigma_u^+(i)\rangle = h_i|(a^3\Pi_u)\rangle + j_i|(^1\Sigma_u^+)\rangle + k_i|(^3\Sigma_u^-)\rangle + l_i|(b^3\Pi_u)\rangle \quad (2)$$

where a_i, b_i, etc., are mixing coefficients. The energies of the spin-orbit states and the mixing coefficients can be determined by diagonalizing the appropriate spin-orbit secular determinants which are given in Table I,[8] where the energies of the singlet and triplet states in the absence of spin-orbit coupling appear along the diagonals, and ζ is the metal spin-orbit coupling constant in the complex.

In order to provide a guide for spectral interpretation, some spin-orbit calculations were made using an approach similar to that used recently by Piepho, Schatz, and McCaffery[9] and by us[10] in the interpretation of MLCT spectra for square-planar $M(CN)_4^{2-}$ complexes. The approach is also the same employed in our earlier study of $Au(CN)_2^-$;[1] however, in that case the calculations are not reliable due to errors in the spin-orbit determinants (see note 8). In these calculations the energies of the singlet and triplet excited states in the absence of spin-orbit coupling, together with the ζ parameter, served as input, and the calculated spin-orbit energies were compared with experimental spectra. The choice of parameters is not completely unrestrained, however, since the placement of the calculated spin-orbit MLCT states must be consistent with the polarized spectral results. Thus the observation of a z-polarized band is only consistent with a $\Sigma_u^+(i)$ state and an xy-polarized band corresponds to a $\Pi_u(i)$ state.

Experimental Spectra. Figure 3 presents spectra at 1.6 K for a thin polycrystalline film of $[(n\text{-}C_4H_9)_4N][Au(CN)_2]$ on quartz. Compared to the 40 K spectra reported earlier,[1] the present measurements reveal considerably more structure, and the major spectral features are much sharper. Some 42 bands are resolved between 40 and 53 kcm^{-1}, and these are tabulated in Table II.

Figure 4 presents polarized electronic spectra and infrared spectra in the region of the CN stretching frequency (inset) for thin single crystals of $[(n\text{-}C_4H_9)_4N][Au(CN)_2]$ grown on optical plates. In both cases strong polarization was found parallel to the crystal extinction directions. However, the crystal face which is developed by the thin crystals could not be determined because all attempts to remove them from the optical plates for x-ray examination resulted in the destruction of the fragile crystals. Therefore some discussion of the relationship between the measured polarized spectra and molecular absorption is necessary. In this connection, the virtually complete polarization of ν_{CN} is significant since the infrared active σ_u^+ CN stretching mode is polarized entirely along the molecular axis (z polarized). This result, together with the parallel arrangement of the linear ions in the crystal determined from diffraction measurements, is consistent with the propagation of the incident polarized light parallel to planes containing the ions. In such a case the absorption of light polarized with the electric vector, **E**, parallel to these planes ($A_\parallel$) is given by eq 3,

$$A_\parallel = A_z \cos\phi + A_{xy} \sin\phi \quad (3)$$

where A_z and A_{xy} are molecular absorptions parallel and perpendicular to the molecular axis, and ϕ is the angle between the molecular axis and **E**. The absorption of light polarized perpendicular to the planes containing the ions is simply given by $A_\perp = A_{xy}$. For the infrared absorption A_{xy} is zero and $A_\parallel = A_z \cos\phi$, but for the electronic spectra $A_\parallel$ will contain contributions from both A_z and A_{xy}, while $A_\perp$ will consist only of the A_{xy} spectrum. This behavior is observed in the experimental spectra: $A_\parallel$ (full curve) shows weak absorptions near the same energy as the intense absorptions in the opposite polarization. If it is assumed that the 47-kcm^{-1} band corresponds to a transition to a Π_u excited state and therefore is exclusively xy polarized ($A_z = 0$), then an estimate of ϕ may

Table II. Spectral Data for $[(n\text{-}C_4H_9)_4N][Au(CN)_2]$

Band no.	$\bar{\nu}$, 10^{-3} cm^{-1} (Relative Absorbance) Unpolarized 1.6 K[a]	Polarized 300 K[b]	Polarization	Assignment	Calcd origin[d]
1	41.237 (0.34)[c]	41.06 (0.13)[c]	$\perp$	$\Pi_u(1)$	41.35
2	41.451 (0.95)[c]	41.55 (2.74)	$\parallel$	$\Sigma_u^+(1)$	41.47
3	41.511 (1.01)			$\Pi_u(1) + \nu_5$	
3a		41.75 (0.93)	$\perp$	$\Pi_u(2)$	41.74
4	42.104 (0.27)[c]			$\Pi_u(2) + \nu_5$	
5	42.239 (0.33)			$\Pi_u(2) + \nu_2$	
6	42.409 (0.47)			$\Pi_u(2) + 2\nu_5$	
7	42.526 (0.50)			$\Pi_u(2) + \nu_5 + \nu_2$	
8	42.680 (0.60)	42.65 (1.33)	$\perp$	$\Pi_u(2) + 3\nu_5$	
8a		42.73 (0.25)	$\parallel$	xy component	
9	42.790 (0.65)			$\Pi_u(2) + 2\nu_5 + \nu_2$	
10	42.973 (0.72)	42.98 (1.24)	$\perp$	$\Pi_u(2) + 4\nu_5$	
10a		43.03 (0.24)	$\parallel$	xy component	
11	43.318 (0.41)			$\Pi_u(1) + \nu_1$	
12	43.516 (0.47)[c]	43.65 (0.36)	$\parallel$	$\Sigma_u^+(1) + \nu_1$	
13	43.745 (0.69)	43.90 (0.97)	$\perp$	$\Pi_u(2) + \nu_1$	
14	44.553 (0.27)	44.70 (0.48)	$\perp$	$\Pi_u(3)$	44.28
15	44.683 (0.26)				
16	44.974 (0.36)[c]			$\Pi_u(3) + \nu_2$	
17	45.045 (0.37)				
18	45.290 (0.46)	45.45 (0.73)	$\perp$	$\Pi_u(1) + 2\nu_1$	
19	45.767 (0.32)[c]				
20	45.872 (0.35)[c]			$\Pi_u(3) + 3\nu_2$	
21	45.998 (0.45)[c]				
22	46.115 (0.64)			$\Pi_u(4)$	46.15
23	46.296 (0.63)[c]			$\Pi_u(3) + 4\nu_2$	
24	46.436 (0.80)[c]				
24a		46.78 (0.59)	$\parallel$	xy component	
25	46.707 (1.28)	46.95 (3.2)	$\perp$	$\Pi_u(3) + \nu_1$ $\Pi_u(3) + 5\nu_2$	
26	47.125 (0.69)[c]			$\Pi_u(3) + 6\nu_2$	
27	47.710 (0.72)[c]			$\Pi_u(4) + n\nu_2$	
28	48.170 (1.42)			$\Pi_u(4) + \nu_1$	
29	48.333 (1.32)[c]			$\Pi_u(4) + \nu_1 + \nu'$	
30	48.603 (1.24)			$\Pi_u(4) + \nu_1 + \nu_2$	
31	48.751 (1.22)[c]			$\Pi_u(3) + 2\nu_1$	
32	49.140 (0.98)[c]			$\Sigma_u^+(3) + n\nu_5$	49.02
33	49.371 (1.10)[c]			$\Sigma_u^+(3) + (n+1)\nu_5$	
34	49.603 (1.26)[c]			$\Sigma_u^+(3) + (n+2)\nu_5$	
35	49.850 (1.37)			$\Sigma_u^+(3) + (n+3)\nu_5$	
36	50.556 (1.98)			$\Pi_u(5)$	50.63
37	50.916 (1.78)			$\Pi_u(5) + \nu_2$	
38	51.295 (1.32)[c]			$\Pi_u(5) + 2\nu_2$	
39	51.680 (1.24)			$\Pi_u(5) + 3\nu_2$	
40	52.049 (1.21)[c]			$\Pi_u(5) + 4\nu_2$	
41	52.219 (1.39)			$\Pi_u(6)$	52.30
42	52.632 (1.27)			$\Pi_u(5) + \nu_1$	

[a] Polycrystalline film on quartz. [b] Single crystal on quartz. [c] Shoulder. [d] Spin-orbit states; input parameters given in caption of Figure 5.

be made. It is easy to show that for this case $A_\parallel/A_\perp = \sin\phi$, and the ratio for the 47-kcm^{-1} band gives a value for ϕ of ca. 10°. This implies that the incident light is nearly normal to the molecular axis. Thus the $A_\perp$ spectrum (dashed curve) is interpreted as xy-polarized absorption corresponding to Π_u excited states, while the intense band at 41.55 kcm^{-1} and a weaker one at 43.65 kcm^{-1} in the $A_\parallel$ spectrum (full curve) are interpreted as z-polarized absorption corresponding to transitions to Σ_u^+ excited states. All other weak features in the $A_\parallel$ spectrum can be traced to an xy component. The strong xy polarization of the 47-kcm^{-1} band is compatible with the earlier MCD results[1] which shows a distinct, positive A term for this band indicating the presence of a degenerate Π_u excited state.

Spectral Assignments. The numerous structured bands in the 1.6 K spectra (Figure 3) indicate that transitions to the electronic excited states are accompanied by vibrational excitation. In order to compare the MLCT spin-orbit states with these spectra, vibrational progressions must be identified and the various electronic origins located, since the spin-orbit model can only describe differences between ground and excited electronic states. In this connection it is worthwhile to note that if the molecular ion is assumed to remain linear in the excited states, then only totally symmetric σ_g^+ vibrational modes are expected to be observed. From Raman measurements[11] on the ground state of $Au(CN)_2^-$ the two σ_g^+ modes are ν_1 2164 cm^{-1} (CN stretch) and ν_2 452 cm^{-1} (AuC stretch). However, it might be anticipated that both modes will be reduced in energy in MLCT excited states since electronic excitations will populate antibonding orbitals.

An analysis of the 1.6 K spectra indicates that a number of the structured features can be interpreted in terms of ν_1 and ν_2 vibrations with frequencies reduced slightly from ground state values. Assignments based on this analysis are set forth

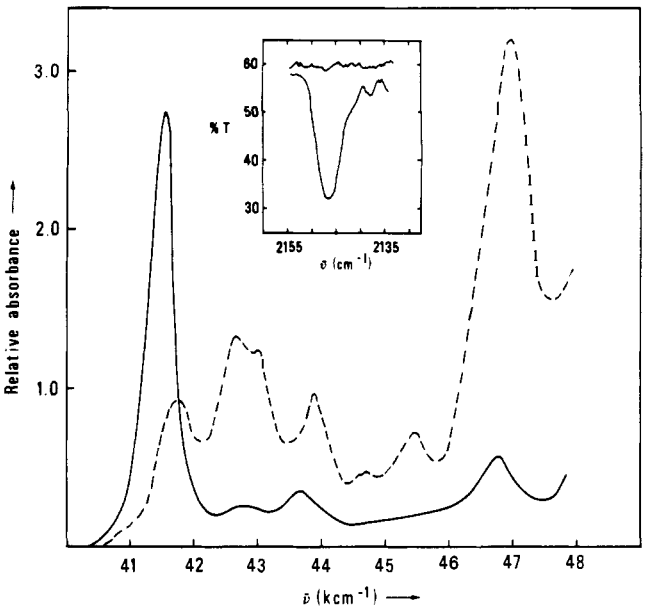

Figure 4. Polarized infrared and electronic spectra for thin single crystals of $[(n\text{-}C_4H_9)_4N][Au(CN)_2]$ grown on optical plates. Inset: infrared absorption in the cyanide stretching region: $A_\perp$, upper curve; $A_\parallel$, lower curve. Electronic spectra: $A_\parallel$, —; $A_\perp$, - - -.

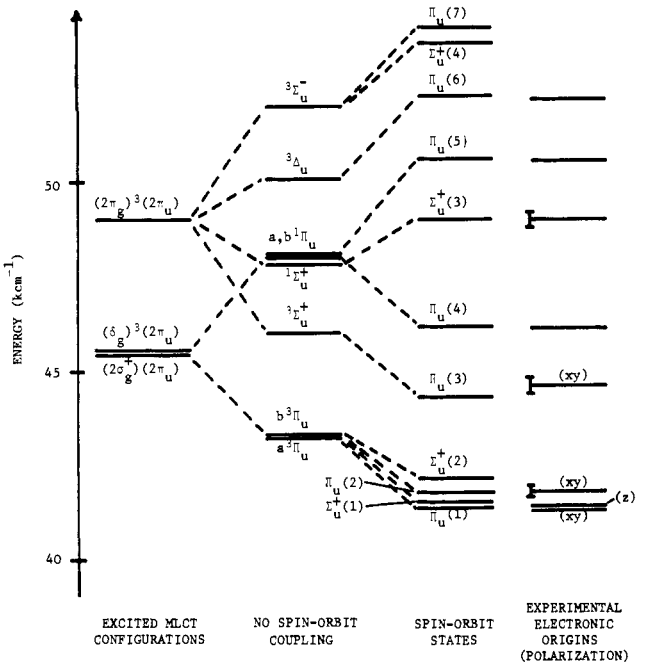

Figure 5. Spin-orbit states for $Au(CN)_2^-$. Input parameters for the calculated states (in kcm^{-1}): $\zeta = 3.0$; $a^1\Pi_u$, 48.0; $a^3\Pi_u$, 43.3; $^1\Sigma_u^+$, 47.8; $^3\Sigma_u^+$, 46.0; $^3\Delta_u$, 50.1; $^3\Sigma_u^-$, 52.0; $b^3\Pi_u$, 43.3; $b^1\Pi_u$, 48.0. Experimental spectral data from 1.6 K measurements (Figure 3); error bars indicate uncertainty in the location of the electronic origins; polarization of lower energy bands indicated in parentheses.

in Table II. The symmetries of the electronic states for transitions below 47 kcm^{-1} are taken to be consistent with the polarized spectra at 300 K (Figure 4), while symmetries for transitions at higher energy were inferred from spin-orbit calculations (see below). Thus for example, the intense, *z*-polarized band near 41.5 kcm^{-1} (band 2, Table II) is assigned as the origin of a transition to a Σ_u^+ state, while a weaker *z*-polarized band 2100 cm^{-1} higher in energy at 43.6 kcm^{-1} (band 12) is interpreted as one quantum of ν_1 built on the 41.5-kcm^{-1} origin. The *xy*-polarized shoulder at 41.06 kcm^{-1} (band 1) is assigned as a Π_u origin, and a short progression in ν_1 is identified in the 1.6 K spectra involving bands 1, 11, and 18 ($\Delta\nu$ = 2080 and 1970 cm^{-1}, respectively). The structure in the intense band at 46.7 kcm^{-1} in the 1.6 K spectra is also interpreted in terms of a Π_u origin, located near 44.5-44.7 kcm^{-1} in the vicinity of bands 14 and 15; progressions in both ν_1 and ν_2 appear, though the lower energy members of the ν_2 progression are split into two bands separated by 130 ± 20 cm^{-1}. The origin of this splitting is not known, but may be due to reduced site symmetry in the polycrystalline sample. The value of ν_2 is 418 ± 10 cm^{-1} (six members located) and the value of ν_1 is 2030 ± 10 cm^{-1} (three members). Another Π_u origin is presumed at the intense 50.556 kcm^{-1} maximum in the 1.6 K spectra (band 36). A progression on the high energy side of this band gives a somewhat low value for ν_2 (370 ± 11 cm^{-1}, five members), but band 42 is interpreted as one quantum of ν_1 (2076 cm^{-1}) higher in energy than the origin.

The structure in the 42-43-kcm^{-1} region (bands 4-10) and in the 49-50-kcm^{-1} region (bands 32-35) shows progressions in a lower frequency than ν_2. In the former case a progression can be identified with a frequency of 292 ± 15 cm^{-1} (four members) based on a Π_u origin located near 41.7-41.8 kcm^{-1}. This progression is complicated, however, and there appears to be another active vibrational mode present as well, perhaps ν_2. In the 49-50-kcm^{-1} region the separation between adjacent bands is 239 ± 6 cm^{-1} (four members, bands 32-35). The $Au(CN)_2^-$ ion also possesses a π_g bending mode, ν_5, which has a ground state frequency of 305 cm^{-1}.[11] If the ν_5 bending vibration is responsible for the structure in these regions, then the observation of this nontotally symmetric mode indicates that the linear ion must be bent slightly in the electronic excited states involved. Finally, the shoulder at 48.333 kcm^{-1} (band 29) is only 163 cm^{-1} higher in energy than the 48.170 kcm^{-1} maximum and may be another low frequency vibration, ν', but it cannot clearly be identified with one of the normal modes of $Au(CN)_2^-$ and is too high in energy to be attributed to lattice phonons. A satisfactory explanation for this band is not available at this time.

As part of the interpretation of the structured features in the 1.6 K spectra, electronic origins were tentatively located either at the lowest energy observed vibrational component or where overlapping bands were present, one vibrational quantum of ν_2 or ν_5 lower in energy. These origins served as the basis for a comparison with calculated MLCT spin-orbit states. The results of the calculations, together with the successful input parameters, are given in Figure 5. The calculated MLCT spin-orbit origins for the $\Pi_u(i)$ and $\Sigma_u^+(i)$ states are included in Table II for comparison with the experimental spectra. Spin-orbit mixing coefficients are given in Table III; the coefficients of the singlet component(s) in the various MLCT states favorably reflect the observed spectral intensities. Input parameters significantly different from those given in Figure 5 failed to produce a spectral fit consistent with both the low resolution features in the polarized spectra at 300 K and those observed at higher resolution in the 1.6 K spectra. Further these results agree *qualitatively* with the MCD spectra obtained earlier.[1] Prominent A terms are observed for the intense bands whose origins are located at 44.5 and 46.12 kcm^{-1} and assigned as $\Pi_u(i)$ states. More than qualitative consideration of the MCD results, however, is difficult because the solution MCD spectra are comparatively low resolution and considerable, overlapping structure is observed at higher resolution. Higher resolution MCD data would clearly be desirable here.

Bonding and Electronic Structure in $Au(CN)_2^-$. It is gratifying that the simple spin-orbit MLCT model involving a single π^* virtual orbital works as well as it does to distribute excited states for $Au(CN)_2^-$ consistent with experimental spectra. It may be remarked here that both values of ζ and the singlet-triplet energy differences between states arising from the same configuration are quite comparable to those found

Table III. Calculated Spin-Orbit Eigenvalues and Mixing Coefficients

		Π_u States						
State	Energy (kcm^{-1})	$a^1\Pi_u$	$a^3\Pi_u$	$^3\Sigma_u^+$	$^3\Delta_u$	$^3\Sigma_u^-$	$b^3\Pi_u$	$b^1\Pi_u$
$\Pi_u(1)$	41.35	0.044	−0.557i	−0.394	−0.152	−0.173	0.681i	0.214
$\Pi_u(2)$	41.74	0.008	0.691i	0.131	0.217	−0.149	0.597i	0.281
$\Pi_u(3)$	44.28	−0.488	−0.209i	0.677	−0.311	0.125	0.067i	0.377
$\Pi_u(4)$	46.15	0.646	−0.161i	0.248	0.319	0.449	−0.083i	0.430
$\Pi_u(5)$	50.63	−0.175	0.222i	−0.515	−0.224	0.053	−0.368i	0.682
$\Pi_u(6)$	52.30	−0.415	−0.271i	−0.052	0.811	−0.231	−0.103i	0.171
$\Pi_u(7)$	54.16	−0.373	0.140i	−0.200	0.149	0.839	0.149i	0.229

	Σ_u^+ States				
State	Energy (kcm^{-1})	$a^3\Pi_u$	$^1\Sigma_u^+$	$^3\Sigma_u^-$	$b^3\Pi_u$
$\Sigma_u^+(1)$	41.47	0.606	−0.473	−0.046i	0.636
$\Sigma_u^+(2)$	42.12	0.698	−0.004	0.321i	0.639
$\Sigma_u^+(3)$	49.02	0.229	0.821	0.317i	−0.415
$\Sigma_u^+(4)$	53.68	−0.302	−0.318	0.891i	−0.115

successful in the analogous MLCT treatment of the square-planar $Pt(CN)_4^{2-}$ and the related $Pt(CNR)_4^{2+}$ complexes.[10,12] Thus it appears that spin-orbit effects and electronic repulsions in MLCT states are quite comparable between the $5d^8$ planar and $5d^{10}$ linear cyano complexes, despite the structural difference.

The successful input parameters in the spin-orbit calculations can also provide information concerning the participation of the metal d orbitals in bonding. The estimated relative energies of the excited MLCT configurations (Figure 5) indicate the ordering of the occupied levels as $\sigma_g^+(z^2) \simeq \delta_g(xy, x^2 - y^2) > \pi_g(xz, yz)$, if it is assumed that electron repulsion differences are small. Since the $\delta_g(xy, x^2 - y^2)$ orbital is strictly nonbonding the small stabilization of the $\pi_g(xz, yz)$ orbitals is consistent with metal to ligand π back-bonding, though it must be admitted that the effect is small, the stabilization being only ~3 kcm^{-1}. The participation of the $\sigma_g^+(z^2)$ orbital in σ bonding likewise is very small since the energies of $\sigma_g^+(z^2)$ and $\delta_g(xy, x^2 - y^2)$ are practically the same. It should be pointed out, however, that the energies of the excited MLCT configurations, and therefore the one-electron orbital energies, can only be estimated since the electron repulsions in these configurations are not known completely. Only the singlet and triplet states giving rise to the $\Sigma_u^+(i)$ and $\Pi_u(i)$ spin-orbit states are located by the approach described here. However, even admitting some ignorance of the details of the electronic repulsions in the excited configurations, the total d orbital splitting about the nonbonding $\delta_g(xy, x^2 - y^2)$ orbital is likely less than 3-5 kcm^{-1} indicating quite a small participation of these orbitals in bonding. This conclusion can be compared with recent results from He-I photoelectron spectra for the isoelectronic and isostructural $Hg(CN)_2$ and the related $Hg(CH_3)(CN)$ complexes.[13] Ionizations from the Hg(II) 5d orbitals were found to be distributed over ~2-2.5 eV, approximately the same energy magnitude observed for the spin-orbit splitting of atomic mercury 5d levels. These spectra were interpreted in terms of a comparatively small stabilization of the $\pi_g(xz, yz)$ orbitals relative to the nonbonding $\delta_g(xy, x^2 - y^2)$ orbitals, the stabilization being somewhat larger (~8 kcm^{-1}) than estimated here for $An(CN)_2^-$. However, quantitative comparison should be viewed with caution since in these systems the spin-orbit effects and electron repulsions are of the same magnitude as the orbital splitting. It appears though that the 5d orbital participation in bonding is also comparatively small in these mercury complexes.

The small participation of the filled 5d orbitals in bonding in $Au(CN)_2^-$ (and the Hg(II) complexes as well) is perhaps not too surprising since the 5d level is expected to have nearly a spherical charge distribution and therefore will be substantially "core-like". In other words, the 5d orbitals, when filled, lose their valence character. A similar conclusion can be drawn from the $5d^8$ square-planar $Pt(CN)_4^{2-}$ and $Pt(CNR)_4^{2+}$ complexes.[10,12] The splitting of the *occupied* 5d orbitals (d_{z^2}, d_{xy}, d_{xz}, and d_{yz}) is also small (~5-7 kcm^{-1}), which can be rationalized in terms of "core-like" behavior. In contrast the empty $d_{x^2-y^2}$ orbital is strongly destabilized (~50 kcm^{-1} or more) and is involved to a considerable extent in σ bonding.

Acknowledgments. The author wishes to acknowledge the hospitality of Professor C. J. Ballhausen and the other members of Kemisk Laboratorium IV of the H.C. Orsted Institute, University of Copenhagen, where a portion of this work was done. Acknowledgment is also made to Dr. Sine Larsen of the same laboratory for interpreting the x-ray results and communicating the crystal structure prior to publication.

References and Notes

(1) W. R. Mason, *J. Am. Chem. Soc.*, **95**, 3573 (1973), and references cited therein.
(2) J. R. Perumareddi, A. D. Liehr, and A. W. Adamson, *J. Am. Chem. Soc.*, **85**, 249 (1963).
(3) (a) C. K. Jorgensen, "Absorption Spectra and Chemical Bonding in Complexes", Addison-Wesley, Reading, Mass., 1962, p 198ff; (b) C. K. Jorgensen, *Adv. Chem. Phys.*, **5**, 33 (1963).
(4) O. Glemser and H. Sauer, "Handbook of Preparative Inorganic Chemistry", Vol. II, 2d ed, G. Brauer, Ed., Academic Press, New York, N.Y., 1965, p 1065.
(5) The author is indebted to Fleming Hansen, Kem. Lab. IV, H. C. Orsted Institute for performing the x-ray measurements.
(6) S. Larsen, in preparation.
(7) J. S. Griffith, "Theory of Transition Metal Ions", Cambridge University Press, Cambridge, 1964, Appendix 6.
(8) A number of unfortunate errors were made in the spin–orbit matrix elements reported previously.[1] Consequently the calculated states are not reliable. The basic approach remains valid and useful, however, and the errors in the spin–orbit matrix elements have been corrected in Table I.
(9) S. B. Piepho, P. N. Schatz, and A. J. McCaffery, *J. Am. Chem. Soc.*, **91**, 5994 (1969).
(10) H. Isci and W. R. Mason, *Inorg. Chem.*, **14**, 905 (1975).
(11) L. H. Jones, *J. Chem. Phys.*, **27**, 468 (1975), and *Spectrochim. Acta*, **19**, 1675 (1963).
(12) H. Isci and W. R. Mason, *Inorg. Chem.*, **14**, 913 (1975).
(13) P. Burroughs, S. Evans, A. Hamnett, A. F. Orchard, and N. V. Richardson, *J. Chem. Soc., Chem. Commun.*, 921 (1974).